Ultrasound in Med. & Biol., Vol. 45, No. 8, pp. 1977–1986, 2019

0301-5629/$ - see front matter

https://doi.org/10.1016/j.ultrasmedbio.2019.04.004

● *Original Contribution*

NATURALLY OCCURRING SHEAR WAVES IN HEALTHY VOLUNTEERS AND HYPERTROPHIC CARDIOMYOPATHY PATIENTS

Mihai Strachinaru,* Johan G. Bosch,† Lennart van Gils,* Bas M. van Dalen,* Arend F.L. Schinkel,* Antonius F.W. van der Steen,† Nico de Jong,† Michelle Michels,* Hendrik J. Vos,† and Marcel L. Geleijnse*

* Department of Cardiology, Erasmus MC, Rotterdam, The Netherlands; and † Department of Biomedical Engineering, Erasmus MC, Rotterdam, The Netherlands

(*Received* 17 *September* 2018; *revised* 20 *March* 2019; *in final from* 1 *April* 2019)

Abstract—We apply a high frame rate (over 500 Hz) tissue Doppler method to measure the propagation velocity of naturally occurring shear waves (SW) generated by aortic and mitral valves closure. The aim of this work is to demonstrate clinical relevance. We included 45 healthy volunteers and 43 patients with hypertrophic cardiomyopathy (HCM). The mitral SW (4.68 ± 0.66 m/s) was consistently faster than the aortic (3.51 ± 0.38 m/s) in all volunteers ($p < 0.0001$). In HCM patients, SW velocity correlated with E/e' ratio ($r = 0.346$, $p = 0.04$ for aortic SW and $r = 0.667$, $p = 0.04$ for mitral SW). A subgroup of 20 volunteers were matched for age and gender to 20 HCM patients. In HCM, the mean velocity of 5.1 ± 0.7 m/s for the aortic SW (3.61 ± 0.46 m/s in matched volunteers, $p < 0.0001$) and 6.88 ± 1.12 m/s for the mitral SW(4.65 ± 0.77 m/s in matched volunteers, $p < 0.0001$). A threshold of 4 m/s for the aortic SW correctly classified pathologic myocardium with a sensitivity of 95% and specificity of 90%. Naturally occurring SW can be used to assess differences between normal and pathologic myocardium. (E-mail: m.strachinaru@erasmusmc.nl)

Key Words: **Cardiac shear wave, Cardiac elastography, High frame rate, Tissue Doppler.**

INTRODUCTION

The prevalence of heart failure is approximately 1%–2% of the adult population in developed countries, rising to ≥10% among people >70 y of age (Ponikowski et al. 2016). Heart failure with preserved ejection fraction represents around 50%, but its diagnosis remains challenging. Demonstration of cardiac functional and structural alterations is key to the diagnosis. However, no validated non-invasive gold standard exists for measuring the precise degree of myocardial stiffness (Nagueh et al. 2016).

Stiffness can be estimated *in vivo* by measuring the propagation velocity of externally induced shear waves travelling through a tissue (Shiina et al. 2015), the general principle being that shear waves travel faster in stiffer materials. This *shear wave elastography* can be performed by magnetic resonance or ultrasound imaging. The main present-day applications are liver fibrosis and breast, thyroid, prostate, kidney and lymph node imaging (Shiina et al. 2015; Parker et al. 2011). Several research groups have used external sources to induce shear waves in the myocardium (Bouchard et al. 2009; Pernot et al. 2011; Hollender et al. 2012; Song et al. 2013; Urban et al. 2013; Vejdani-Jahromi et al. 2017), demonstrating that diastolic myocardial stiffness can be determined using ultrasonic shear wave imaging (Villemain et al. 2018a, 2018b). It has been found that shear-like waves also naturally occur in the myocardium after valve closure (Kanai 2009; Brekke et al. 2014), caused by the impulse of the snapping valve on the mitral and aortic annuli which propagates within the cardiac wall. We have recently shown that these waves can be measured with an ultrasound system in regular clinical mode by using high frame rate tissue Doppler imaging (TDI) (Strachinaru et al. 2017).

In this work, we study naturally occurring shear waves in normal volunteers and hypertrophic cardiomyopathy

Address correspondence to: Mihai Strachinaru, Department of Cardiology, Erasmus MC, Office Rg 427, PB 2040, 3000 CA Rotterdam, The Netherlands. E-mail: m.strachinaru@erasmusmc.nl

(HCM) patients, as a pathologic model of increased muscle stiffness and diastolic dysfunction (Villemain et al. 2018a, 2018b; Elliott et al. 2014; Lu et al. 2018; Finocchiaro et al. 2018). The aim was to demonstrate the feasibility in a clinical setting and investigate the potential application of the method for discriminating normal from pathologic myocardium.

METHODS

Study population

This prospective study was conducted in 2016−2017 according to the principles of the Declaration of Helsinki and approved by the Institutional Medical Ethical Committee (MEC-2014-611, MEC-2017-209). Written informed consent was obtained from every participant.

Healthy volunteers aged 18−62 y. Patients were excluded if one or more of the following criteria were present: a history of cardiovascular disease, systemic disease, the finding of cardiac abnormalities during the examination (including QRS duration over 100 ms), cardiovascular risk factors including hypertension (cutoff value 140/90 mm Hg), diabetes mellitus or hypercholesterolemia, having breast implants or being pregnant. Professional athletes or morbidly obese (body mass index [BMI] >40 kg/m^2) were excluded.

HCM patients recruited from the HCM outpatient clinic. Patients were included if they had a definitive diagnosis of HCM (Elliott et al. 2014), regardless of the localization of the most hypertrophic segments (*e.g.*, apical forms were not excluded). Exclusion criteria were associated known coronary artery disease, more than mild valve disease (systolic anterior movement of the mitral valve was not considered as exclusion criterion), prior septal reduction (either surgical or interventional).

Echocardiography

All echocardiographic studies were performed by one experienced sonographer (M.S.). Normal complete echocardiographic studies were performed, including 2-D, Doppler and pulsed-wave TDI of the mitral annulus. The peak velocity of the early diastolic mitral inflow was measured (E wave), as well as the peak early diastolic tissue velocity of the medial mitral annulus in apical four-chambers view (e' wave). Their ratio (E/e') was then calculated as an index of the early diastolic properties of the left ventricle. Tissue velocities of the left ventricular (LV) myocardium were sampled in color tissue Doppler (color TDI) in standard parasternal long axis (PLAX) view using a Philips iE33 system (Philips Medical, Best, The Netherlands) equipped with a S5-1 transducer. As previously described (Strachinaru et al. 2017), we used a clinical color TDI application with a frame rate over 500 Hz, acquiring five separate recordings for each subject, timed to the electrocardiogram in order to obtain two heart beats per recording. The probe was lifted off the chest between recordings and repositioned in order to optimize the image. Typically, the TDI sector had an opening angle of 40°, which at a depth of 6 cm leads to a 4-cm sector width. The 2-D line density was set to minimum, leading to TDI frame rates over 500 Hz (range 500−590 Hz). The TDI videos were stored in Digital Imaging and Communications in Medicine (DICOM) format for offline analysis.

The DICOM TDI loops were processed using Qlab 9 (Philips Medical, Best, The Netherlands); see Figure 1 and Video 1. A shear wave in the color TDI data is detected on the septal wall as a rapid up-and-down tissue displacement, visible in the form of a color shift (red to blue or blue to red depending on the direction). This pattern initiates at the exact visible moment of valve closure which also corresponds to the onset of the heart sounds in the phonocardiography (PCG) signal, and then propagates over the septal wall away from the valve toward the apex.

A curved virtual M-mode line was traced along the centre of the LV wall (Fig. 1a). Its length and direction were predefined by the user. No axial range gate was used. The shear wave source is expected to be at the valvular annulus, as demonstrated in Video 2. Previous literature also mentions that the waves start at the annulus and progresses to the apex (Kanai 2009; Brekke et al. 2014). For consistency, the arrow of the M-mode line always pointed toward the shear wave source, perpendicular to the wave front. The software provides a virtual M-mode map (Fig. 1b), allowing us to manually trace the leading slope of the propagating wave, as previously described (Strachinaru et al. 2017).

The propagation velocity of the wave front was estimated through

$$V_s = D/T, \quad (1)$$

where D is the (user-defined) length of the M-mode line and T is the time the wave travels along the M-mode line. The propagation velocity was averaged over three heartbeats for every subject. The three cycles were freely selected by each observer from the 10 available cycles per subject per exam as the heartbeats where the best visualization of the shear waves could be obtained.

The very short isovolumic times are complex to analyze (Goetz et al. 2005; Golde and Burstin 1970). In order to identify the exact times of valve closure and discriminate shear waves from other events, the acquisitions included a synchronous PCG signal, by using a Fukuda Denshi MA-300 HDS(V) PCG microphone.

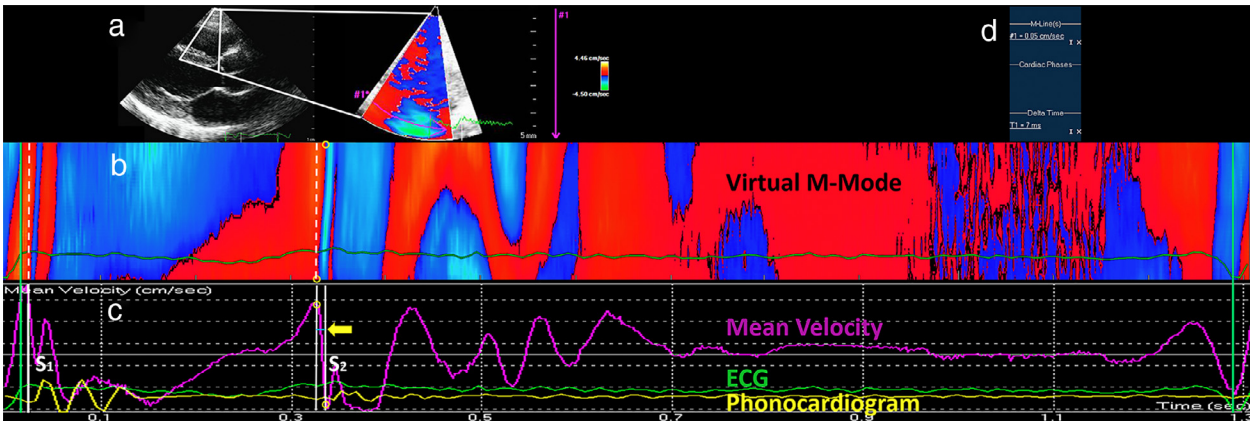

Fig. 1. Detailed view (modified to indicate the main elements) of the data obtained in the study patients by using offline processing in Philips Qlab. (a) Classical PLAX and the focused TDI window over the interventricular septum. The M-mode line is traced mid-wall, pointing toward the shear wave source. (b) Virtual M-mode map of a full heart cycle (reconstructed offline), at 513 Hz, demonstrating the shear waves after mitral and aortic valve closure. The onset of the waves is marked with dotted lines. (c) Mean tissue velocity curve as a function of time (averaged over the M-mode line, this velocity should not be mistaken with the shear wave propagation velocity), synchronous to the ECG (green) and PCG (yellow). The onset of both shear waves is synchronous to the onset of the respective heart sounds (S1, S2). By clicking on the base and the top of the wave front's slope in the color M-mode map (small circles), the program highlights the corresponding points on the mean velocity time curve. The time interval in which the wave occurs is marked with the solid white lines (arrow). (d) Results panel, showing the time interval. PLAX = parasternal long axis; TDI = tissue Doppler imaging; ECG, electrocardiogram; PCG = phonocardiography.

Also, the timing of valve closure from the underlying 2-D data was confirmed by direct visual correlation and anatomic M-mode, using a general post-processing platform (Tomtec Imaging System 4.6, Unterschleissheim, Germany).

Statistical analysis

Distribution of data was checked by using histograms and Shapiro-Wilk tests. Continuous variables were represented as mean ± standard deviation. Categorical data are presented as absolute number and percentages. For comparison of normally distributed continuous variables we used the dependent or independent means *t* test when appropriate. In case of a skewed distribution of continuous variables, the Mann-Whitney *U* test was applied. For comparison of frequencies, the chi-square test or Fisher's exact test was used. Correlations were computed using Pearson's method. Matching of the patients and control groups was done after inclusion, using a propensity score method, with 1:1 nearest neighbor matching according to age and gender.

The relationship between individual variables was estimated using univariate linear regression. Parameters found to be significant or considered relevant based on theoretical assumptions were entered into a multivariate model. Receiver operating characteristic (ROC) analysis was applied in order to evaluate the discriminating power of the method.

Intra-observer variability was evaluated on 11 randomly chosen patients, on the initial recordings with a new measurement set performed by M.S. 2 mo later, blinded to the first result. Inter-observer variability was estimated on the same recordings, between the result of M.S. and the results obtained by a first-time user, with limited prior knowledge of the software application (L. G.), also in a blinded manner. Inter-acquisition variability was evaluated on a different randomly chosen group of 13 study patients, between the initial recordings and a new ultrasound recording set 3 mo later, blinded to the first result. In all variability measurements, the velocity was averaged over three heartbeats for every subject, the reader being allowed to select the best heart cycle from a recording for each measurement. Variability was estimated by using the Bland-Altman method (Bland and Altman 1986).

Every statistical analysis was performed using the Statistical Package for Social Sciences version 21 (IBM SPSS Statistics for Windows, Armonk, NY, USA). Testing was done two-sided and considered significant if the *p* value was smaller than 0.05.

RESULTS

Shear wave behaviour in healthy volunteers

Forty-five healthy volunteers, 64% males, mean age 34 ± 13 underwent a high frame rate ultrasound study (mean TDI frame rate = 516 ± 13 Hz, range 500−590

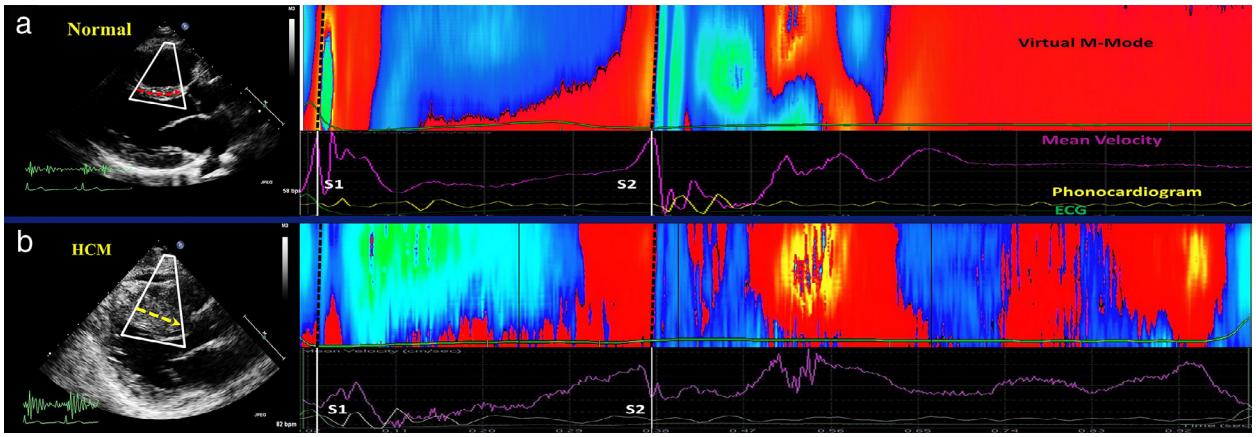

Fig. 2. Shear wave comparison in a normal volunteer and an HCM patient. (a) A M-mode line was traced in the middle of the interventricular septum, resulting in a color M-mode map. Heart sounds are marked with S1 and S2. The slope of the mitral shear wave (synchronous to S1) and of the aortic shear wave (synchronous to S2) are marked with dotted lines. (b) The same diagram, in the case of an HCM patient. In order to compare the slopes of the respective shear waves, the width of the two M-mode maps was adjusted until the respective heart sounds were perfectly aligned (as if the two patients had the same heart rate). HCM = hypertrophic cardiomyopathy.

Hz). Shear waves were visible and quantifiable in the interventricular septum in PLAX view (Fig. 1, Video 1) after mitral valve closure in 40 volunteers (89%) and after aortic valve closure in 42 volunteers (93%). These waves were synchronous to onset of the heart sounds on the PCG and could clearly be linked to the valvular events (Videos 2 and 3).

In PLAX, the mean velocity of the mitral valve shear wave was 4.68 ± 0.66 m/s, range 3.25−6.50 m/s, with a maximal horizontal length of the TDI region of interest of 3−3.5 cm. The mean aortic shear wave velocity was 3.51 ± 0.38 m/s, range 3.00−4.66 m/s. The mitral shear wave was consistently faster than the aortic in all individual patients ($p < 0.0001$).

Male and female volunteers had mitral shear wave velocity values of 4.65 ± 0.62 m/s and 4.72 ± 0.76 m/s ($p = 0.73$), respectively. The aortic shear wave velocity was 3.43 ± 0.32 m/s in males and 3.67 ± 0.45 m/s ($p = 0.05$) in females. There was no correlation between the age of the patients and the aortic shear wave velocity ($R^2 = 0.005$, $p = 0.67$) or the mitral shear wave ($R^2 = 0.006$, $p = 0.64$). Also, no correlation existed with systolic blood pressure ($R^2 = 0.002$, $p = 0.93$ for the mitral shear wave and $R^2 = 0.008$, $p = 0.59$ for the aortic shear wave velocity), diastolic blood pressure ($R^2 = 0.002$, $p = 0.79$ for the mitral shear wave and $R^2 = 0.02$, $p = 0.41$ for the aortic), e' ($R^2 = 0.11$, $p = 0.27$ for the aortic shear wave and $R^2 = 0.04$, $p = 0.51$ for the mitral) and E/e' ratio ($R^2 = 0.14$, $p = 0.21$ for the aortic and $R^2 = 0.01$, $p = 0.9$ for the mitral).

HCM patients

Forty-three HCM patients were also screened and investigated with high frame rate TDI (frame rate of 519 ± 18 Hz, range 500−558 Hz). Their mean age was 51 ± 12, 70% males. Shear waves were visible and quantifiable in the interventricular septum in PLAX view (Fig. 2) after mitral valve closure in 24 patients (56%) and after aortic valve closure in 38 patients (88%).

The mitral shear wave had a mean velocity of 6.7 ± 1.3 m/s. No correlation was found between the mitral shear wave velocity and age ($R^2 = 0.04$, $p = 0.53$), systolic blood pressure ($R^2 = 0.04$, $p = 0.57$), diastolic blood pressure ($R^2 = 0.01$, $p = 0.89$) and e' ($R^2 = 0.09$, $p = 0.37$). The aortic shear wave mean velocity was 5.2 ± 0.8 m/s. No correlation was found for the aortic shear wave with age ($R^2 = 0.02$, $p = 0.45$), systolic blood pressure ($R^2 = 0.03$, $p = 0.32$), diastolic blood pressure ($R^2 = 0.01$, $p = 0.48$) and e' ($R^2 = 0.07$, $p = 0.12$).

The E/e' ratio was significantly correlated with the aortic shear wave velocity ($r = 0.346$, $R^2 = 0.119$, $p = 0.04$) and mitral shear wave velocity ($r = 0.667$, $R^2 = 0.444$, $p = 0.04$).

Factors influencing the shear wave velocity in the two study groups (unmatched)

Given the very good feasibility of the aortic shear wave detection in both groups, the clinical and echocardiographic parameters were compared to the aortic shear wave velocity by univariate and multivariate regression in each separate group. In normal volunteers (Table 1), male gender was the only significant parameter influencing the aortic shear wave velocity, both in univariate and multivariate regression.

In HCM patients, male gender and E/e' ratio were found to significantly influence the aortic shear wave velocity in univariate analysis. In the multivariate model,

Table 1. Parameters influencing the aortic shear wave velocity in normal volunteers and HCM patients in univariate and multivariate regression analysis

	Normal volunteers N = 45				HCM patients N = 43			
	Univariate		*Multivariate*		*Univariate*		*Multivariate*	
	B	*p*	*B*	*p*	*B*	*p*	*B*	*p*
Male sex	−0.240	0.05	−0.524	**0.01**	0.538	0.05	0.509	0.06
Age	0.002	0.67			0.008	0.45		
BMI	−0.026	0.16			−0.023	0.38		
Systolic blood pressure	0.003	0.59			−0.007	0.32		
Diastolic blood pressure	0.008	0.41			−0.008	0.48		
Septal thickness	0.012	0.77	0.110	0.12	0.05	0.08	0.026	0.4
e’	−0.044	0.27			−0.108	0.12		
E/e’	0.075	0.21	0.009	0.87	0.42	**0.04**	0.039	**0.045**

HCM = hypertrophic cardiomyopathy; BMI = body mass index.
Significant *p* values (<0.05) are highlighted in bold.

the only parameter significantly influencing the aortic shear wave velocity was the E/e’ ratio.

Matching for comparative analysis

Matching the two groups for age and gender resulted in a group of 20 normal volunteers and 20 HCM patients. The matched patients’ baseline characteristics and echocardiographic results are shown in Table 2.

There were significant differences in BMI, diastolic blood pressure, septal thickness, e’ and E/e’ ratio between the baseline features of these groups. The velocity of the aortic shear wave (Figs. 2 and 3) was significantly higher in the HCM group (mean value = 5.13 ± 0.68 m/s, range 3.75−6.94 m/s) compared with the normal (3.61 ± 0.45 m/s, range 3.10−4.66 m/s, $p < 0.0001$). Mitral shear wave velocity was also significantly higher in HCM (6.88 ± 1.12 m/s, range 5.45−8.91 m/s) than in the normal group (Figs. 2 and 3), (4.65 ± 0.77, range 3.25−6.50 m/s, $p < 0.0001$).

ROC analysis for detecting the pathologic myocardium (HCM) by the aortic shear wave velocity showed an area under the curve of 0.98, with a sensitivity of 95% and specificity of 90% for a cutoff value of 4 m/s (Fig. 4). The septal thickness used as reference had an area under the curve of 0.95. Figure 4 illustrates patients’ classification according to the two thresholds (septal thickness >15 mm and aortic shear wave velocity >4 m/s). Note that two patients had normal septal thickness and apical hypertrophy, and two others were diagnosed through family screening (in which maximum wall thickness threshold = 13 mm for diagnosis of HCM).[15]

Table 2. Comparison between matched normal individuals and HCM patients, ordered into demographic characteristics, echocardiographic parameters and study results, respectively

Parameter	Normal volunteers N = 20	HCM patients N = 20	*p*
Age (y)	45 ± 13	48 ± 13	0.47
Male gender (%)	60	70	0.51
Height (m)	176 ± 10	176 ± 9	0.96
Weight (kg)	76 ± 15	84 ± 16	0.09
BMI	24 ± 4	27 ± 4	**0.04**
Systolic blood pressure (mm Hg)	119 ± 15	131 ± 24	0.06
Diastolic blood pressure (mm Hg)	71 ± 8	80 ± 11	**0.01**
Septal thickness (mm)	9 ± 1	17 ± 5	<**0.0001**
Septal e’ (cm/s)	8.3 ± 1	5.5 ± 2	<**0.0001**
Septal E/e’	8 ± 1	17 ± 9	<**0.0001**
Frame rate parasternal (s^{-1})	511 ± 27	511 ± 20	0.98
Aortic shear wave velocity parasternal (m/s)	3.61 ± 0.45	5.13 ± 0.68	<**0.0001**
Mitral shear wave velocity parasternal (m/s)	4.65 ± 0.77	6.88 ± 1.12	<**0.0001**

HCM = hypertrophic cardiomyopathy; BMI = body mass index.
Significant *p* values (<0.05) are highlighted in bold.

Variability

For intra-observer variability (no = 11 readings of parasternal aortic valve shear wave), the first reading displayed a mean velocity of 3.74 ± 0.59 m/s. At the second reading, the mean value was 3.72 ± 1.04 m/s ($p = 0.86$). The mean difference was 0.03 ± 0.52 m/s. The limits of agreement (LOA) were −0.99 to +1.05 m/s (Fig. 5a).

For the inter-observer variability (Fig. 5b), the mean value of the shear wave velocity obtained by the second observer was 3.51 ± 1.21 m/s ($p = 0.29$). The mean difference between observers was −0.23 ± 0.69 m/s (LOA = −1.12 to +1.59 m/s).

Test-retest (inter-acquisition) variability was estimated on a group of 13 volunteers (Fig. 5c). The velocity of the parasternal aortic valve shear wave velocity was 3.51 ± 0.42 on the first recording, and the second imaging recording taken 3 mo later had a velocity of 3.52 ± 0.35 ($p = 0.95$). The mean difference was −0.006 ± 0.37 m/s (LOA = −0.74 to +0.73 m/s).

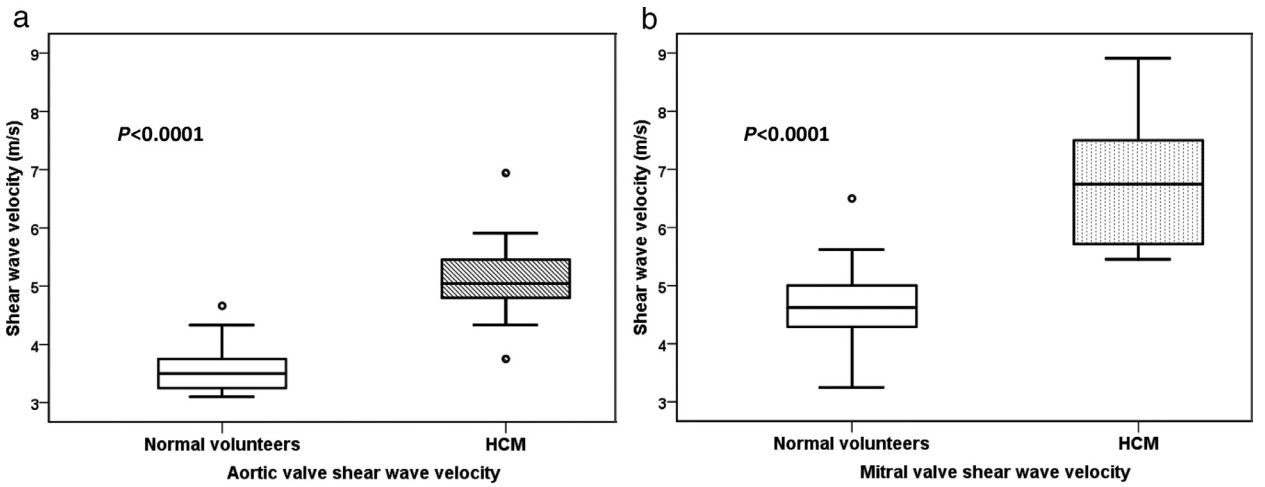

Fig. 3. Velocity values for the aortic shear wave (a) and mitral shear wave (b) in normal volunteers and HCM patients. The shear waves are significantly faster in HCM, with no significant overlap of the velocity ranges. HCM = hypertrophic cardiomyopathy.

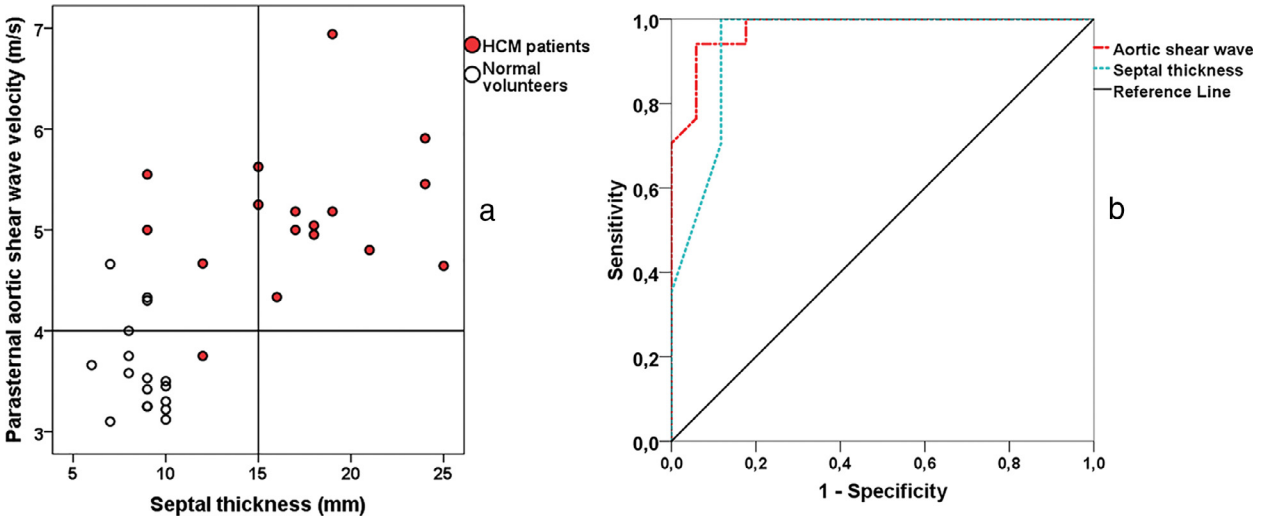

Fig. 4. (a) Study patients classified according to the septal thickness (X axis, vertical line at the 15 mm threshold) and aortic shear wave velocity (Y axis, horizontal line at the threshold value of 4 m/s determined by ROC analysis). Note that HCM patients with normal or intermediate septal thickness were correctly classified by the 4 m/s threshold. (b) ROC curves for detecting normal versus abnormal myocardium by the septal thickness versus the aortic shear wave velocity. ROC = receiver operating characteristic; HCM = hypertrophic cardiomyopathy.

DISCUSSION

This prospective study shows that (i) assessment of naturally occurring shear wave velocities is feasible in both normal volunteers and patients, using a high frame rate TDI application available on a clinical echocardiography scanner in regular clinical mode; (ii) the velocity of these shear waves is significantly higher in pathologic myocardium (HCM patients); and (iii) the velocity of these waves correlates with the E/e' ratio in HCM patients.

In several studies, the detection of these fast phenomena in the heart has been described (Pernot et al. 2011; Hollender et al. 2012; Song et al. 2013; Urban et al. 2013; Vejdani-Jahromi et al. 2017; Villemain et al. 2018a, 2018b; Brekke et al. 2014; Kanai et al. *2000*; Kanai 2005, 2009; Couade et al. 2011; Pislaru et al. 2017) using experimental systems or modified software. We have already demonstrated that by tuning the relationship between the depth of the image, the 2-D line density, sector width and the TDI field of view sufficient time resolution can be achieved, allowing visualization

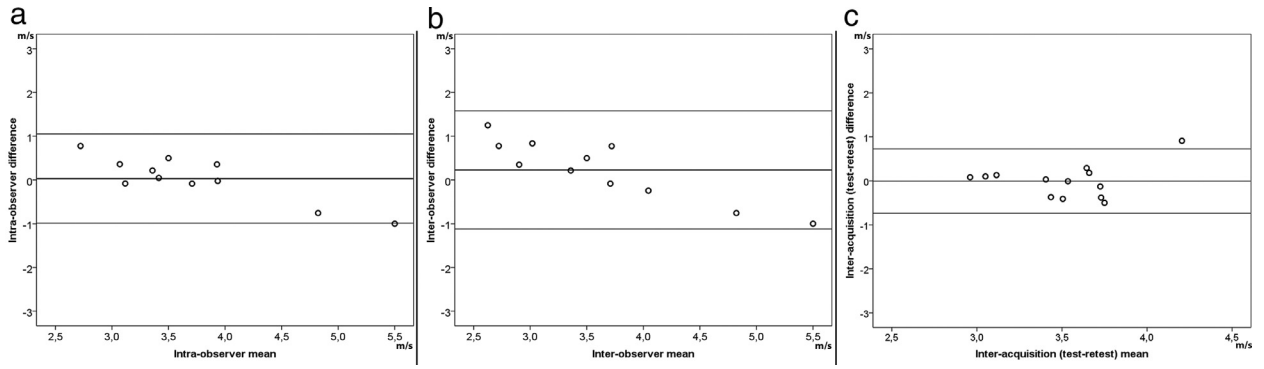

Fig. 5. Variability of the shear wave velocity measurement, illustrated by Bland-Altman plots. The central horizontal line represents the mean difference and external lines the limits of agreement. (a) intraobserver variability; (b) interobserver variability; (c) test-retest (inter-acquisition) variability.

of the shear waves with a conventional clinical scanner (Strachinaru et al. 2017).

The LV isovolumetric periods are very short (30−100 ms). However, several mechanical, electrical and hemodynamic events take place during this time (Goetz et al. 2005; Golde and Burstin 1970; Konofagou and Provost 2012; Costet et al. 2014). In patients with normal atrio-ventricular and intraventricular conduction, the first component of the two heart sounds is the valvular component: mitral (for the first heart sound) and aortic (for the second heart sound), respectively (Leatham 1954), and thus synchronous with the onset of the fast shear waves generated by the closure of the same valves (Remme 2008). Propagation delay for the PCG tracings is negligible due to the difference in velocity (1540 m/s for sound waves vs. 1−10 m/s for shear waves). In order to clearly delineate the shear waves from other phenomena, the TDI recordings were timed on the PCG. For both aortic and mitral shear waves, the origin and propagation could be documented and linked to the valvular events by using synchronized TDI, 2-D, M-mode and PCG tracings (Videos 2 and 3).

The shear wave is associated with particle vibration with a main component perpendicular to the direction of propagation. In the parasternal position, this main component is parallel to the direction of the ultrasound beam. Therefore, as already demonstrated (Strachinaru et al. 2017), a TDI system would be most sensitive for shear waves traveling through the interventricular septal wall in a *parasternal* view, rather than in an *apical* view. A slight angulation in the parasternal position between the particle vibration and the ultrasound beam will reduce the apparent amplitude of the shear wave. However, unlike conventional TDI where the magnitude of the axial TDI velocity is measured, it will not affect the apparent lateral propagation velocity of the wave pattern, which is the primary outcome of our measurement.

On the other hand, a misalignment between the 2-D imaging plane and the source of the waves can lead to overestimation in the propagation velocity estimation. A classical PLAX lies strictly perpendicular to the mitral annulus and cuts through the middle of the aortic annulus, reducing this risk of misalignment. Also, an angulation of the M-mode line with respect to the true central line of the septum might induce an intra-scan variability estimated to 5%−10% (Keijzer et al. 2018).

The effects of myocardial fiber structure on the wave velocity can be quite significant, which may result in anisotropic shear wave propagation as observed with radiation force-induced shear wave elastography (Villemain et al. 2018a, 2018b; Urban et al. 2016). Yet, the relatively low oscillation frequency (order 50−100 Hz) of the waves might reduce the effect of the fiber structure (Song et al. 2016, Urban et al. 2016). Furthermore, viscous loss will introduce dispersion (Bercoff et al. 2004), and the finite wall thickness may lead to dispersive Lamb waves (Kanai 2005), although a previous animal study has shown only a mild dispersion of the waves after aortic valve closure (Vos et al. 2017). For simplicity, we have chosen the mid-wall position, presumably having the highest consistency in placement. Further clinical studies are warranted in order to detect and characterize the possible variation in velocity along and across the LV wall.

Moreover, the stiffness itself, hence the shear modulus, varies in time throughout the cardiac cycle (Kanai 2005; Couade et al. 2011), thus changing the instantaneous shear wave speed. Yet, we track the leading edge of the wave which propagates over relatively short distances and very short intervals ($T < 12$ ms), as imposed by the limited opening of the TDI field of view. Therefore, this variation could be neglected and the propagation assumed to be linear.

The precision of the measurement is restricted by the field of view (represented by M-mode length D) and frame rate. Variance in T is caused by rounding off to integer frame intervals. The precision can be improved by averaging multiple recordings. Also a larger image sector and higher frame rate (order 1000 frames/s) would reduce the variance in the measurements (Strachinaru et al. 2017). We found a larger variance for the mitral (range of 3.25 m/s) than for the aortic shear wave velocity (range of 1.66 m/s) in healthy volunteers. Several of the following arguments could be evoked: (i) the higher velocity of the wave inherently produces higher variability (Strachinaru et al. 2017); (ii) the lower transvalvular gradient over the mitral valve leads to lower wave amplitudes; (iii) the very complex mechanical and electrical events in early systole (Konofagou and Provost 2012) may lead to errors in shear wave quantification during this time instance; and (iv) the relative position of the shear wave source (mitral annulus) to the anteroseptal wall in parasternal position may result in overestimation, because the source of the wave is not strictly inside the measurement plane, as mentioned before.

The propagation velocity of the aortic valve closure wave in our healthy patients is lower than that found in a group of 10 human patients by Brekke et al. (2014) (5.41 $\pm$ 1.28 m/s), or in animal studies (Hollender et al. 2012; Vos et al. 2017). We speculate that the difference is originating from the different detection method and probe positioning: parasternal in our study in agreement with Kanai (2005) as opposed to apical in the study by Brekke et al (2014). Interestingly, the propagation velocity of the aortic shear waves may be influenced by gender as demonstrated in our healthy volunteers group. The difference, although statistically significant, seems minor in terms of absolute numbers (3.43 $\pm$ 0.32 m/s in males and 3.67 $\pm$ 0.45 m/s, $p = 0.05$ in females). Full characterization of the behaviour of naturally occurring shear waves in the heart remains to be investigated in future studies.

In animal model studies, the propagation of the mitral valve shear wave has been found to be lower than the aortic (Vos et al. 2017). The opposite finding in the human heart cannot be explained by differences in electromechanical activation (Konofagou and Provost 2012; Costet et al. 2014). It is however noteworthy that the animal studies were performed under sedation, which has a notable impact on the loading conditions of the left ventricle.

The physiology of the isovolumetric periods remains challenging. The instantaneous LV wall stiffness has several components: an active component due to muscle contraction, a parietal tension derived from Laplace's law and an inert elasticity of the fully relaxed wall (Pernot et al. 2011; Remme et al. 2008). The instantaneous value of stiffness is the sum of these dynamic and static components. Our detection method is able to record naturally occurring shear waves during two moments in the cardiac cycle: one in early systole (mitral valve shear wave) and the other in early diastole (aortic valve shear wave). Although none of these moments corresponds to a truly diastolic state (full relaxation of the LV myocardium), the significant difference found in our study between normal and non-compliant myocardium (as demonstrated by the highly significant difference in e'), as well as the positive correlation with the E/e' ratio suggests that the naturally occurring shear waves could be clinically relevant in estimating myocardial stiffness. However, future studies are needed to elucidate the relation between the shear wave propagation velocities measured during the isovolumetric periods and the actual compliance of the left ventricle.

A positive correlation was found in HCM patients between the velocities of the naturally occurring shear waves (both mitral and aortic) and the E/e' ratio. This observation is consistent with the hypothesis that naturally occurring shear wave velocity is correlated to the degree of diastolic dysfunction as defined by the E/e' ratio.

Clinical application and future directions

Pediatric and adult HCM patients have already been tested by using shear wave imaging (Villemain et al. 2018a, 2018b). These investigations were performed with ultrafast special equipment and externally induced shear waves, and demonstrated a significantly higher shear wave velocity (difference of 1.5 m/s) in HCM patients with proven decreased LV compliance and higher degree of fibrosis. In our study, there was also a very significant and similar difference (1.5 m/s for aortic shear wave and 2.1 m/s for the mitral) between shear wave velocities in normal and pathologic myocardium, with minimal overlap and an excellent discriminating power. Patients with normal septal thickness but apical hypertrophy were also correctly classified by using a 4 m/s threshold (Fig. 4), as well as patients with septal thickness ranging from 13−15 mm diagnosed through screening. This suggests that the method could be used to discriminate pathologic myocardium regardless of the septal thickness. However, the ROC analysis was performed on limited numbers and only on one extreme pathology. Therefore, we refrain from computing and reporting general limits for the normal myocardium. Also, we noticed a lower feasibility for the mitral shear wave in HCM patients than in healthy volunteers, and therefore the same analysis for mitral shear wave velocity was considered less meaningful.

A diagnostic index that uses both waves would theoretically be interesting, but requires a systematic

detection of both shear waves in the same heart cycle. This was not always possible in our patients, for three reasons: first that shear waves velocities were calculated by choosing the heart cycles where the visualization of the respective wave was optimal, but not necessarily the cycle where both shear waves were visualized; second that in some patients only one of the shear waves was quantifiable; and third, in color TDI the velocity scale for optimally detecting the mitral shear wave was generally different (lower) than the one needed to detect the aortic shear wave. Also, because of the abnormal distribution of variables in the total group (two extremes: normal individuals with low shear wave velocities and HCM patients with much higher shear wave velocities), a linear correlation analysis between the two shear waves could not be performed. Such a correlation should be investigated over a continuum of normality and pathology.

This technique provides a possible quantitative assessment of myocardial stiffness during the isovolumic periods. The potential clinical benefit is major: from early detection of diastolic abnormalities and improved characterization of heart failure with preserved ejection fraction to a possible new endpoint in future studies of pharmacologic innovations (Cikes et al. 2014; Voigt 2018). Further studies with a longitudinal design are needed in order to demonstrate the prognostic implications.

Study limitations

This is a monocentric study on a small population, so the results cannot be directly extrapolated to the general population. Another important limitation is the lack of ground truth. Invasive stiffness measurement in volunteers remains difficult (because of practical and ethical reasons), and no validated non-invasive imaging modality is available for the study of cardiac stiffness *in vivo* (Lancelotti et al. 2017). Prior clinical studies have, however, linked the significant difference in shear wave velocities between HCM patients and normal volunteers to a difference in LV compliance and stiffness (Villemain et al. 2018a, 2018b). Other confounding factors could also influence this correlation (blood pressure, filling conditions). Before a direct quantification of stiffness can be done, these confounding factors need to be investigated. The added value of the naturally occurring shear waves' velocity as an independent diagnostic parameter remains to be shown in a larger population and a wider array of pathology.

A wave with a velocity of 5 m/s travels over 3.5 cm in 7 ms. At 500 Hz the time resolution is 2 ms, so such a fast wave would be captured in three to five separate frames. This time resolution can be insufficient when trying to quantify velocities over 5 m/s over very short distances. However, the inter- and intra-observer agreement were good, with differences of the same magnitude as the inter-measures variability, as reflected by the standard deviation. This variability is also significantly lower than the difference found between normal and pathologic LV. We foresee that the advancement in technology, with even higher frame rates becoming available, and/or changes in data processing will allow a reduction in measurement error.

Manual tracking as allowed by the manufacturer-designed software is time consuming and prone to errors, demonstrated by the larger inter-observer variability. Therefore, new research should focus on a robust method of automated velocity tracking from the DICOM frames.

The lack of correlation with age, blood pressure and E/e' in normal volunteers should be interpreted with caution. The absence of age extremes (under 18 and over 65) and the overall normal blood pressure leads to a tight distribution of data around a normal value, limiting the yield of such analyses.

CONCLUSION

Naturally occurring shear waves in the *in vivo* human heart can be imaged using a standard clinical TDI application. The study demonstrates that quantification of these shear waves is feasible and can be used to assess differences between normal and pathologic myocardium, opening the way to a new method of estimating myocardial stiffness.

Acknowledgments—This work was supported by the Domain Applied and Engineering Sciences—Dutch Heart Foundation partnership program "Earlier recognition of cardiovascular diseases" with project number 14740, which is (partly) financed by the Netherlands Organization for Scientific Research.

SUPPLEMENTARY MATERIALS

Supplementary material associated with this article can be found in the online version at doi:10.1016/j.ultrasmedbio.2019.04.004.

REFERENCES

Bercoff J, Tanter M, Muller M, Fink M. The role of viscosity in the impulse diffraction field of elastic waves induced by the acoustic radiation force. IEEE Trans Ultrason Ferroelectr Freq Control 2004;51:1523–1536.

Bland JM, Altman DG. Statistical methods for assessing agreement between two methods of clinical measurement. Lancet 1986;1:307–310.

Bouchard RR, Hsu SJ, Wolf PD, Trahey GE. In vivo cardiac, acoustic-radiation-force-driven, shear wave velocimetry. Ultrason Imaging 2009;31:201–213.

Brekke B, Nilsen LC, Lund J, Torp H, Bjastad T, Amundsen BH, Stoylen A, Aase SA. Ultra-high frame rate tissue Doppler imaging. Ultrasound Med Biol 2014;40:222–231.

Cikes M, Tong L, Sutherland GR, D'hooge J. Ultrafast cardiac ultrasound imaging: Technical principles, applications, and clinical benefits. JACC Cardiovasc Imaging 2014;7:812–823.

Costet A, Provost J, Gambhir A, Bobkov Y, Danilo P, Jr, Boink GJ, Rosen MR, Konofagou EE. Electromechanical wave imaging of biologically and electrically paced canine hearts in vivo. Ultrasound Med Biol 2014;40:177–187.

Couade M, Pernot M, Messas E, Bel A, Ba M, Hagege A, Fink M, Tanter M. In vivo quantitative mapping of myocardium stiffening and transmural anisotropy during the cardiac cycle. IEEE Trans Med Imaging 2011;30:295–305.

Elliott PM, Anastasakis A, Borger MA, Borggrefe M, Cecchi F, Charron P, Hagege AA, Lafont A, Limongelli G, Mahrholdt H, McKenna WJ, Mogensen J, Nihoyannopoulos P, Nistri S, Pieper PG, Pieske B, Rapezzi C, Rutten FH, Tillmanns C, Watkins H. 2014 ESC Guidelines on diagnosis and management of hypertrophic cardiomyopathy: The Task Force for the Diagnosis and Management of Hypertrophic Cardiomyopathy of the European Society of Cardiology (ESC). Eur Heart J 2014;35:2733–2779.

Finocchiaro G, Dhutia H, D'Silva A, Malhotra A, Sheikh N, Narain R, Ensam B, Papatheodorou S, Tome M, Sharma R, Papadakis M, Sharma S. Role of Doppler diastolic parameters in differentiating physiological left ventricular hypertrophy from hypertrophic cardiomyopathy. J Am Soc Echocardiogr 2018;31:606–613.

Goetz WA, Lansac E, Lim HS, Weber PA, Duran CM. Left ventricular endocardial longitudinal and transverse changes during isovolumic contraction and relaxation: A challenge. Am J Physiol Heart Circ Physiol 2005;289:H196–H201.

Golde D, Burstin L. Systolic phases of the cardiac cycle in children. Circulation 1970;42:1029–1036.

Hollender PJ, Wolf PD, Goswami R, Trahey GE. Intracardiac echocardiography measurement of dynamic myocardial stiffness with shear wave velocimetry. Ultrasound Med Biol 2012;38:1271–1283.

Kanai H, Yonechi S, Susukida I, Koiwa Y, Kamada H, Tanaka M. Onset of pulsatile waves in the heart walls at end-systole. Ultrasonics 2000;38:405–411.

Kanai H. Propagation of spontaneously actuated pulsive vibration in human heart wall and in vivo viscoelasticity estimation. IEEE Trans Ultrason Ferroelectr Freq Control 2005;52:1931–1942.

Kanai H. Propagation of vibration caused by electrical excitation in the normal human heart. Ultrasound Med Biol 2009;35:936–948.

Keijzer L, Bosch JG, Verweij M, de Jong N, Vos HJ. Intra-scan variability of natural shear wave measurements. IEEE IUS 2018;1720–1724.

Konofagou EE, Provost J. Electromechanical wave imaging for noninvasive mapping of the 3 D electrical activation sequence in canines and humans in vivo. J Biomech 2012;45:856–864.

Lancellotti P, Galderisi M, Edvardsen T, Donal E, Goliasch G, Cardim N, Magne J, Laginha S, Hagendorff A, Haland TF, Aaberge L, Martinez C, Rapacciuolo A, Santoro C, Ilardi F, Postolache A, Dulgheru R, Mateescu AD, Beladan CC, Deleanu D, Marchetta S, Auffret V, Schwammenthal E, Habib G, Popescu BA. Echo-Doppler estimation of left ventricular filling pressure: Results of the multicentre EACVI Euro-Filling study. Eur Heart J Cardiovasc Imaging 2017;18:961–968.

Leatham A. Splitting of the first and second heart sounds. Lancet 1954;267(6839):607.

Lu DY, Haileselassie B, Ventoulis I, Liu HY, Liang HY, Pozios I, Canepa M, Phillip S, Abraham MR, Abraham T. E/e' ratio and outcome prediction in hypertrophic cardiomyopathy: The influence of outflow tract obstruction. Eur Heart J Cardiovasc Imaging 2018;19:101–107.

Nagueh SF, Smiseth OA, Appleton CP, Byrd BF, 3rd, Dokainish H, Edvardsen T, Flachskampf FA, Gillebert TC, Klein AL, Lancellotti P, Marino P, Oh JK, Popescu BA, Waggoner AD. Recommendations for the evaluation of left ventricular diastolic function by echocardiography: An update from the American Society of Echocardiography and the European Association of Cardiovascular Imaging. J Am Soc Echocardiogr 2016;29:277–314.

Parker KJ, Doyley MM, Rubens DJ. Imaging the elastic properties of tissue: The 20 year perspective. Phys Med Biol 2011;56:R1–R29.

Pernot M, Couade M, Mateo P, Crozatier B, Fischmeister R, Tanter M. Real-time assessment of myocardial contractility using shear wave imaging. J Am Coll Cardiol 2011;58:65–72.

Pislaru C, Alashry MM, Thaden JJ, Pellikka PA, Enriquez-Sarano M, Pislaru SV. Intrinsic wave propagation of myocardial stretch, a new tool to evaluate myocardial stiffness: A pilot study in patients with aortic stenosis and mitral regurgitation. J Am Soc Echocardiogr 2017;30:1070–1080.

Ponikowski P, Voors AA, Anker SD, Bueno H, Cleland JGF, Coats AJS, Falk V, González-Juanatey JR, Harjola VP, Jankowska EA, Jessup M, Linde C, Nihoyannopoulos P, Parissis JT, Pieske B, Riley JP, Rosano GMC, Ruilope LM, Ruschitzka F, Rutten FH, van der Meer P. 2016 ESC Guidelines for the diagnosis and treatment of acute and chronic heart failure: The task force for the diagnosis and treatment of acute and chronic heart failure of the European Society of Cardiology (ESC). Eur Heart J 2016;37:2129–2200.

Remme EW, Lyseggen E, Helle-Valle T, Opdahl A, Pettersen E, Vartdal T, Ragnarsson A, Ljosland M, Ihlen H, Edvardsen T, Smiseth OA. Mechanisms of preejection and postejection velocity spikes in left ventricular myocardium: Interaction between wall deformation and valve events. Circulation 2008;118:373–380.

Shiina T, Nightingale KR, Palmeri ML, Hall TJ, Bamber JC, Barr RG, Castera L, Choi BI, Chou YH, Cosgrove D, Dietrich CF, Ding H, Amy D, Farrokh A, Ferraioli G, Filice C, Friedrich-Rust M, Nakashima K, Schafer F, Sporea I, Suzuki S, Wilson S, Kudo M. WFUMB guidelines and recommendations for clinical use of ultrasound elastography: Part 1: Basic principles and terminology. Ultrasound Med Biol 2015;41:1126–1147.

Song P, Zhao H, Urban MW, Manduca A, Pislaru SV, Kinnick RR, Pislaru C, Greenleaf JF, Chen S. Improved shear wave motion detection using pulse-inversion harmonic imaging with a phased array transducer. IEEE Trans Med Imaging 2013;32:2299–2310.

Song P, Bi X, Mellema DC, Manduca A, Urban MW, Greenleaf JF, Chen S. Quantitative assessment of left ventricular diastolic stiffness using cardiac shear wave elastography: A pilot study. J Ultrasound Med 2016;35:1419–1427.

Strachinaru M, Bosch JG, van Dalen BM, van Gils L, van der Steen AFW, de Jong N, Geleijnse ML, Vos HJ. Cardiac shear wave elastography using a clinical ultrasound system. Ultrasound Med Biol 2017;43:1596–1606.

Urban MW, Pislaru C, Nenadic IZ, Kinnick RR, Greenleaf JF. Measurement of viscoelastic properties of in vivo swine myocardium using lamb wave dispersion ultrasound vibrometry (LDUV). IEEE Trans Med Imaging 2013;32:247–261.

Urban MW, Qiang B, Song P, Nenadic IZ, Chen S, Greenleaf JF. Investigation of the effects of myocardial anisotropy for shear wave elastography using impulsive force and harmonic vibration. Phys Med Biol 2016;61:365–382.

Vejdani-Jahromi M, Freedman J, Nagle M, Kim YJ, Trahey GE, Wolf PD. Quantifying myocardial contractility changes using ultrasound-based shear wave elastography. J Am Soc Echocardiogr 2017;30:90–96.

Villemain O, Correia M, Khraiche D, Podetti I, Meot M, Legendre A, Tanter M, Bonnet D, Pernot M. Myocardial stiffness assessment using shear wave imaging in pediatric hypertrophic cardiomyopathy. JACC Cardiovasc Imaging 2018a;11:779–781.

Villemain O, Correia M, Mousseaux E, Baranger J, Zarka S, Podetti I, Soulat G, Damy T, Hagège A, Tanter M, Pernot M, Messas E. Myocardial stiffness evaluation using noninvasive shear wave imaging in healthy and hypertrophic cardiomyopathic adults. JACC Cardiovasc Imaging 2018b. doi: 10.1016/j.jcmg.2018.02.002. [Epub ahead of print].

Voigt JU. Direct stiffness measurements by echocardiography: Does the search for the holy grail come to an end? JACC Cardiovasc Imaging 2018. doi: 10.1016/j.jcmg.2018.02.004. (in press).

Vos HJ, van Dalen BM, Heinonen I, Bosch JG, Sorop O, Duncker DJ, van der Steen AF, de Jong N. Cardiac shear wave velocity detection in the porcine heart. Ultrasound Med Biol 2017;43:753–764.